

Characterization of Mixing in a Coaxial Jet Mixer
for Nanoparticle Fabrication

by

Laura Gilson

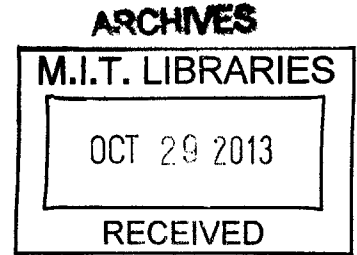
Submitted to the
Department of Mechanical Engineering
in Partial Fulfillment of the Requirements for the Degree of

Bachelor of Science

at the

Massachusetts Institute of Technology

June 2013



© 2013 Massachusetts Institute of Technology. All rights reserved

Signature of Author

Department of Mechanical Engineering
May 10, 2013

Certified by

Rohit Karnik
Associate Professor of Mechanical Engineering
Thesis Supervisor

Accepted by

Anette Hosoi
Professor of Mechanical Engineering
Undergraduate Officer

Characterization of Mixing in a Coaxial Jet Mixer for Nanoparticle Fabrication

by

Laura Gilson

Submitted to the Department of Mechanical Engineering
on May 10, 2013 in Partial Fulfillment of the
Requirements for the Degree of

Bachelor of Science in Mechanical Engineering

ABSTRACT

Mixing in a micro-scale coaxial turbulent jet mixer for the fabrication of nanoparticles for drug delivery was experimentally characterized. Rapid mixing due to turbulence offers improved control of nanoparticle production over conventional bulk nanoprecipitation methods.

Mixing time was determined based on photographs of mixing of an acidic solution and a basic solution in the device, with phenolphthalein used as an indicator of the extent of mixing. The average Reynolds number and velocity ratio were varied. The velocity ratio varied between 0.1 and 10. The Reynolds number varied between 200 and 1800. Mixing times on the order of 1 to 50 ms were measured in the device. The mixing time was found to be proportional to average velocity to the $-3/2$ power. The data showed some agreement with predicted mixing time based on the EDD model for turbulent micromixing in the jetting regime.

Thesis Supervisor: Rohit Karnik

Title: Associate Professor of Mechanical Engineering

Acknowledgements

The author would like to thank Professor Rohit Karnik and Jong-Min Lim for their guidance and assistance with this project.

Table of Contents

Abstract	3
Acknowledgements	5
Table of Contents	7
List of Figures	9
1. Introduction	11
1.1 Nanoparticles in Medicine	11
1.2 Methods for Fabrication of Nanoparticles	12
1.3 The Coaxial Jet Mixer	12
2. Predicting mixing time	14
2.1 Problem Summary	14
2.2 Mixing due to flow focusing	15
2.3 Turbulent Mixing	16
3. Testing mixing time predictions	16
3.1 Experimental procedure	16
3.2 Image Analysis	18
3.3 Determining Mixing Time	19
4. Results and Discussion	19
4.1 Mixing Time	19
4.3 Future Work	21
5. Conclusion	22
7. Bibliography	23

List of Figures

Figure 1:	Illustration of the coaxial jet mixer	13
Figure 2:	Flow through the coaxial jet mixer	14
Figure 3:	Photograph of experimental setup	17
Figure 4:	Methods for determining mixing time	18
Figure 5:	Plot of mixing time versus Reynolds number	20
Figure 6:	Plot of non-dimensionalized mixing time versus Reynolds number	21

1. Introduction

Nanoparticles have shown promise as a vehicle for delivering drugs to target cells within the body. In comparison to bulk nanoprecipitation methods, microfluidic devices for nanoparticle fabrication have demonstrated a good ability to control physicochemical properties of therapeutic nanoparticles, which strongly affect their *in vivo* fate.^{1,2}

A significant hurdle in the further clinical acceptance of nanoparticles for medical applications is the development of consistent, high-throughput devices for nanoparticle fabrication.³ This study focuses on the mixing of two fluids in a novel coaxial turbulent jet mixer for the production of nanoparticles, which allows high throughput and control of the product's physicochemical properties. We characterize the mixing time in the device as a function of the net Reynolds number and the velocity ratio of the input flows.

1.1 Nanoparticles in Medicine

Nanoparticles are well-suited to medical applications because they are on the same scale as the biological processes typically disrupted by disease.⁴ In particular, nanoparticles have much to offer in the areas of drug delivery and imaging. Loaded liposomes and polymeric nanoparticles have been used to deliver drugs to specific types of cells,⁵ while metallic nanoparticles, especially iron oxide nanoparticles, have been developed for use as contrast agents for magnetic resonance imaging (MRI)⁶.

One key advantage of nanoparticles is that they can be engineered to target specific cells. This is important both for drug delivery and imaging applications. Many drugs, especially cancer-fighting drugs, are toxic to healthy cells and diseased cells alike, so the maximum dosage is limited by the need to minimize side effects such as the necrosis of healthy cells.⁷ A method of drug delivery that specifically targets diseased cells practically circumvents that limit. Targeting is also useful for imaging, where the ability to visually distinguish between healthy and diseased tissue is advantageous for diagnostic purposes.⁶

Physicochemical properties of nanoparticles determine their ability to target diseased cells. The enhanced permeability and retention (EPR) effect describes cancerous tissue's tendency to allow greater permeation of large molecules from the bloodstream, and to

retain these molecules for a longer time, relative to healthy tissue. Cancer cells can thus be passively targeted based on nanoparticles' size.⁵ Cells can also be actively targeted using surface modifications that enhance binding to or uptake by specific kinds of cells.³

The size of nanoparticles in such applications partially determines their effectiveness. The size of iron oxide nanoparticles used as MRI contrast agents governs the speed of uptake by organs, so the nanoparticles' size is engineered to suit the imaging of specific organs and structures.⁶ Size also contributes to the fate of nanoparticles used for targeted drug delivery.⁵ Consequently, good control of the size and size distribution of nanoparticles is required of nanoparticle production processes.

1.2 Methods for Fabrication of Nanoparticles

A wide range of processes are used for the fabrication of nanoparticles. Two-step methods first emulsify and then form nanoparticles from the emulsion. Emulsification may be carried out by a variety of methods and technologies, such as droplet extrusion or the use of a colloidal mill. Nanoparticles can then be formed from the emulsified droplets by such methods as evaporation of solvent and polymerization of the nanoparticle.⁸

A simpler, less energy-intensive method for forming nanoparticles is nanoprecipitation, which adds a polymer in its non-solvent to the polymer's solvent, causing polymer nanoparticles to precipitate out in a simple and repeatable way.⁹ This process may be done in bulk, but microfluidic devices offer greater control over the mixing process and the resulting particles.³ Microfluidic mixing devices using flow focusing¹ and impinging jets^{10,11} have been proposed and studied.

1.3 The Coaxial Jet Mixer

The coaxial jet mixing device under consideration here is shown below in Figure 1. Its geometry is simple: two flows enter the device through coaxial tubes, and mixing occurs at the termination of the inner tube. The behavior of the device depends on the velocities of the flows into the device. The mixer may function as an axially symmetric 3-dimensional flow-focusing device, where a focused inner flow is mixed with the outer flow by diffusion. Alternatively, if the velocities are high enough, turbulence may induce rapid mixing. Rapid mixing is desirable in such devices because it accelerates throughput,

allows the fabrication of more complicated composite nanoparticles, and reduces the need for nanoparticle storage.¹²

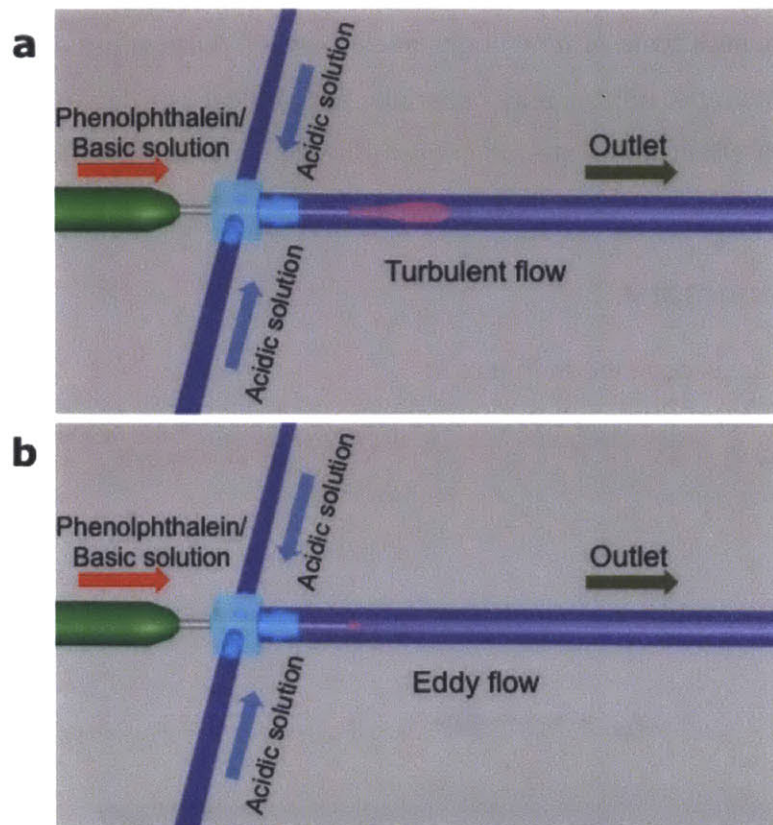


Figure 1: Schematic illustration of the coaxial jet mixer, showing two distinct flow regimes: (a) turbulent flow and (b) eddy flow. Mixing occurs after the inner flow is injected into the coaxial outer flow.

Mixing time depends on the fluid properties and input flow velocities, but the way in which the mixing time may scale with input parameters is difficult to determine analytically. Baldyga and Bourne demonstrate a computational approach to a similar problem.¹³ This project examines experimental data on mixing time in the device for a range of velocity ratios and Reynolds numbers, in order to characterize mixing in the device.

2. Predicting mixing time

Mixing is the process of homogenizing the distribution of one material in another. As mixing occurs, the length scale of inhomogeneities shrinks.¹³ Depending on the Reynolds number and flow rate ratio, mixing may occur due to turbulence or due to flow focusing. To determine which effect dominates, it is useful to compare the expected mixing time for each of these regimes.

2.1 Problem Summary

The flow in the device is depicted in Figure 2.

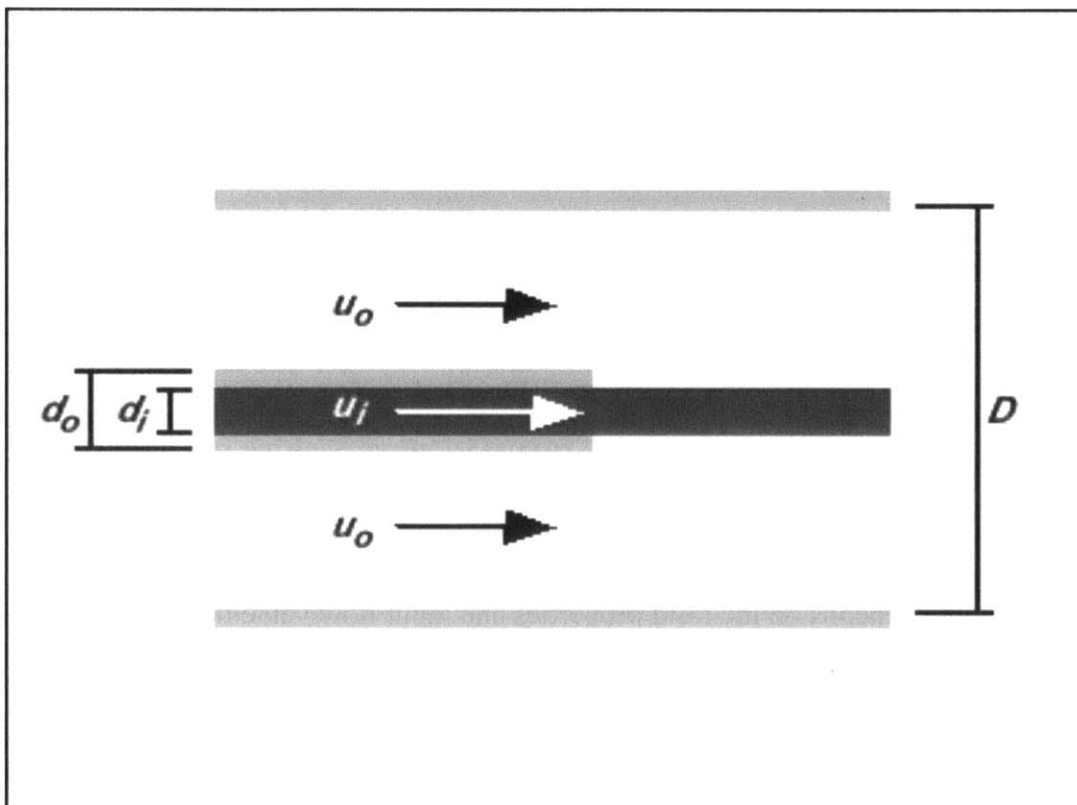


Figure 2: Flow through the coaxial jet mixer.

In the case examined here, the two fluids have approximately the same density ρ and kinematic viscosity ν . The kinematic viscosity of the water-ethanol mixture used in the experiments (see Section 3.1) was assumed to be $2.589 \times 10^{-6} \frac{\text{m}^2}{\text{s}}$, based on the work of Khattab et al.¹⁴ The device geometry is described by D , the diameter of the outer tube,

and d_i and d_o , the inner diameter and outer diameter, respectively, of the inner tube. The device's length is much greater than its diameter or any observed mixing length, except in some cases when the flow is not turbulent. The two input velocities U_i and U_o may be fully defined by setting the dimensionless velocity ratio R_u and average-velocity Reynolds number Re_{ave} where

$$R_u = \frac{U_i}{U_o} \quad (1)$$

and

$$Re_{ave} = \frac{u_{ave}D}{\nu} \quad (2)$$

Here u_{ave} is the average velocity over a cross-section of the device:

$$u_{ave} = \frac{(D^2 - d_o^2)U_o + d_i^2U_i}{D^2} \quad (3)$$

2.2 Mixing due to flow focusing

Flow focusing is expected to be the dominant mixing phenomenon when the velocity ratio and Reynolds number are small. Extending the correlation for mixing time in a two-dimensional flow focusing device given by Karnik et al.,¹ we find a correlation for the mixing time due to flow focusing in a cylindrical flow focusing device:

$$\tau_{mix} \sim \frac{d_f^2}{4D}, \quad (4)$$

where d_f is the focused diameter of the inner flow, and D is the mass diffusivity.

The focused diameter of the inner flow is

$$d_f = d_i \sqrt{\frac{u_i}{u_{ave}}} \quad (5)$$

from the conservation of mass.

2.3 Turbulent Mixing

Description of mixing is complicated by the fact that length scales on different orders of magnitude contribute to the problem.¹⁵ The engulfment, deformation, diffusion (EDD) turbulent micromixing model considers mixing to be a process in which unmixed fluid is entrained into turbulent vortices, the vortices stir the fluid at their characteristic frequency, creating a layered structure, and, once the layers are small enough, molecular diffusion finishes the mixing process.¹³ The characteristic time for this process is given as

$$\tau_{\omega} \approx 12 \left(\frac{\nu}{\langle \epsilon \rangle} \right)^{\frac{1}{2}} \quad (6)$$

where $\langle \epsilon \rangle$ is the average turbulent kinetic energy dissipation rate. The energy dissipation rate in the core of a pipe flow can be estimated as

$$\epsilon_c = 0.0668 \frac{\bar{u}^3}{Re^{1/4} D} \quad (7)$$

where \bar{u} is the average velocity in the axial direction.¹⁶ The Reynolds number used in this analysis is the average-velocity Reynolds number Re_{ave} .

3. Testing mixing time predictions

3.1 Experimental procedure

The experimental device was a coaxial jet mixer shown previously in Figure 1. The inner flow was injected through a 23-Gauge needle into the coaxial outer flow through 1/8"-diameter tubing. The inner diameter and outer diameter of the needle were 0.6414 mm and 0.337 mm, respectively. Three syringe pumps drove the inner and outer flows at a set inner and outer velocity. For each velocity ratio, which ranged from $\frac{U_i}{U_o} = 0.1$ to 10, tests were carried out at an outer velocity varying from 100 to 1000 mm/s.

The mixing of an acidic outer flow with a basic inner flow was tracked using the pH indicator phenolphthalein, which is purple in basic solutions and becomes transparent in neutral or acidic solutions. The inner flow solution contained by volume 10% 1N NaOH, 23.3% phenolphthalein solution, and 66.7% ethanol. The phenolphthalein solution

contained 1% phenolphthalein (mass per volume) in water. The outer flow solution contained by volume 10% HCl, 23.3% water and 66.7% ethanol.

As mixing occurred during testing, the HCl neutralized the NaOH, and the color of the fluid indicated the degree of mixing: an unmixed jet appeared purple, and as mixing enabled a change in pH, the color weakened until the jet became indistinguishable in color from the surrounding fluid.

The mixing in the device was photographed several times for each combination of velocities. A right angle prism mirror placed next to the device, shown in Figure 3 enabled photographs to capture a view from above the device and a view from the side of the device simultaneously.

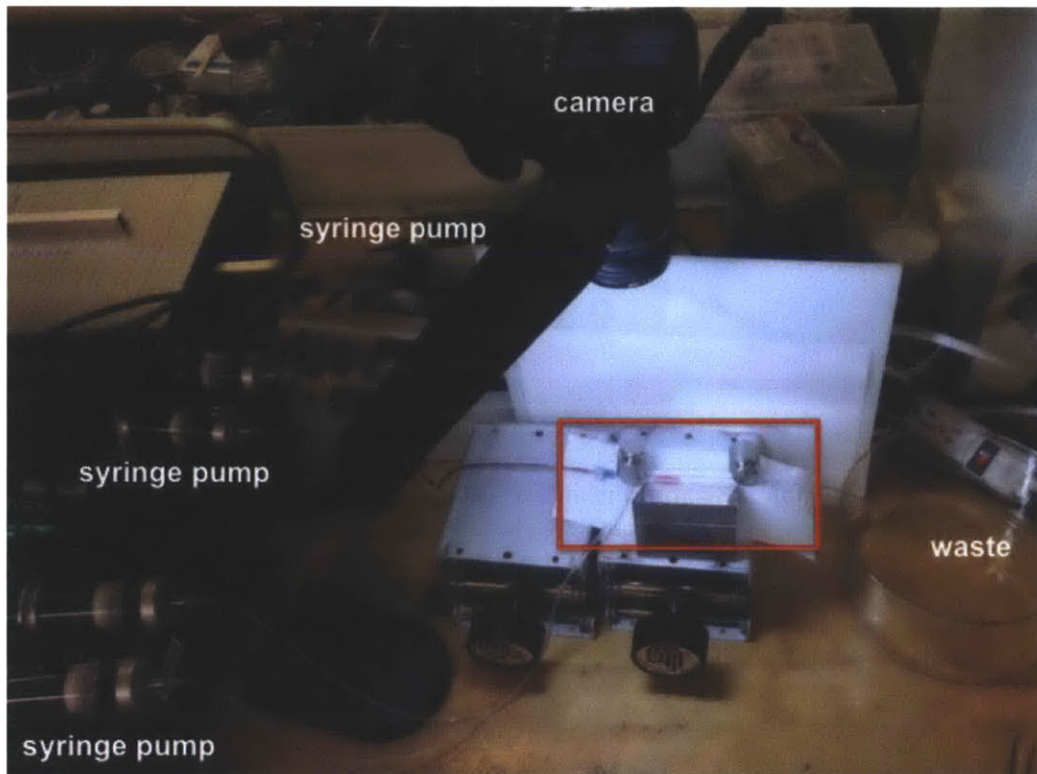


Figure 3: Photograph of experimental setup. Flow is driven by three syringe pumps. The device is boxed in red. The right-angle prism mirror is located just below the device.

These photographs support the assumption that the density of the two flows is almost the same: the vertical drift of the mixing flow is very small, indicating negligible buoyant forces and thus a negligible difference in the densities of the two flows.

3.2 Image Analysis

A characteristic mixing length was determined from photos of the device taken under different flow conditions (velocity ratio and average velocity were varied systematically). Since the phenolphthalein appears fuchsia, the complementary green channel of the RGB images was analyzed in ImageJ to extract a mixing length for each photo, as shown in Figure 4.

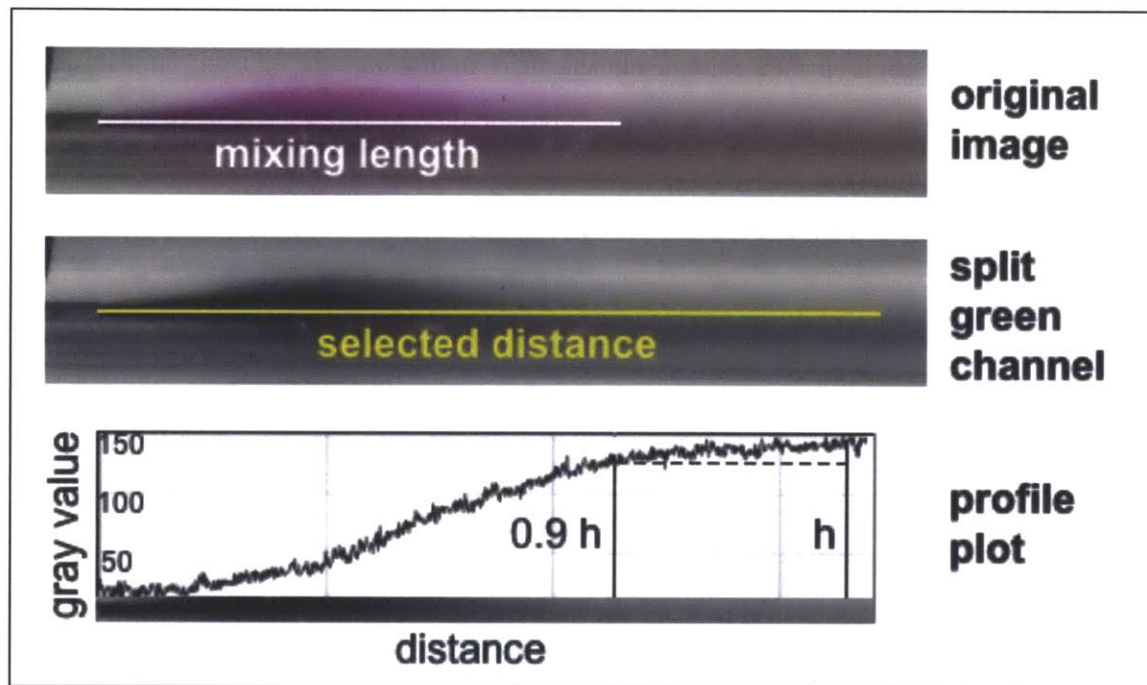


Figure 4: Method for determining mixing time. The mixing length is shown superimposed on the original image (top). This mixing length is the length at which the gray value of the RGB green channel is 90% of its maximum value h , both relative to the initial value (bottom). The selected distance is chosen somewhere after the flow is visibly fully mixed, but before any major change in the glare in the photographs.

The intensity profile of the green color channel of the image was found along the centerline of the jet, and the mixing length L was defined as the length at which the difference between it and the beginning of the jet was 90% of the intensity difference between the completely mixed flow far downstream and the beginning of the jet.

No mixing time was estimated for the tests for which the flow was still unmixed at the rightmost edge of the image.

3.3 Determining Mixing Time

From the mixing lengths, determined in as described above, mixing times were estimated using the following equation:

$$\tau_{mix} = \frac{L}{u_{ave}}. \quad (8)$$

The use of (8) assumes that the particles being mixed travel at u_{ave} as their average velocity throughout the mixing process. This is not strictly true: though the particles' speed far downstream is u_{ave} , they enter the device at the inner flow velocity U_i . If U_i and u_{ave} are not equal, any one particle's time-average velocity will not be u_{ave} . However, this assumption allows us to make simplified statements about the scaling of the mixing in the devices.

4. Results and Discussion

The mixing time was plotted and compared to the predictions of the EDD model described above.

4.1 Mixing Time

The mixing times are plotted as a function of Re_{ave} for each velocity ratio in Figure 5.

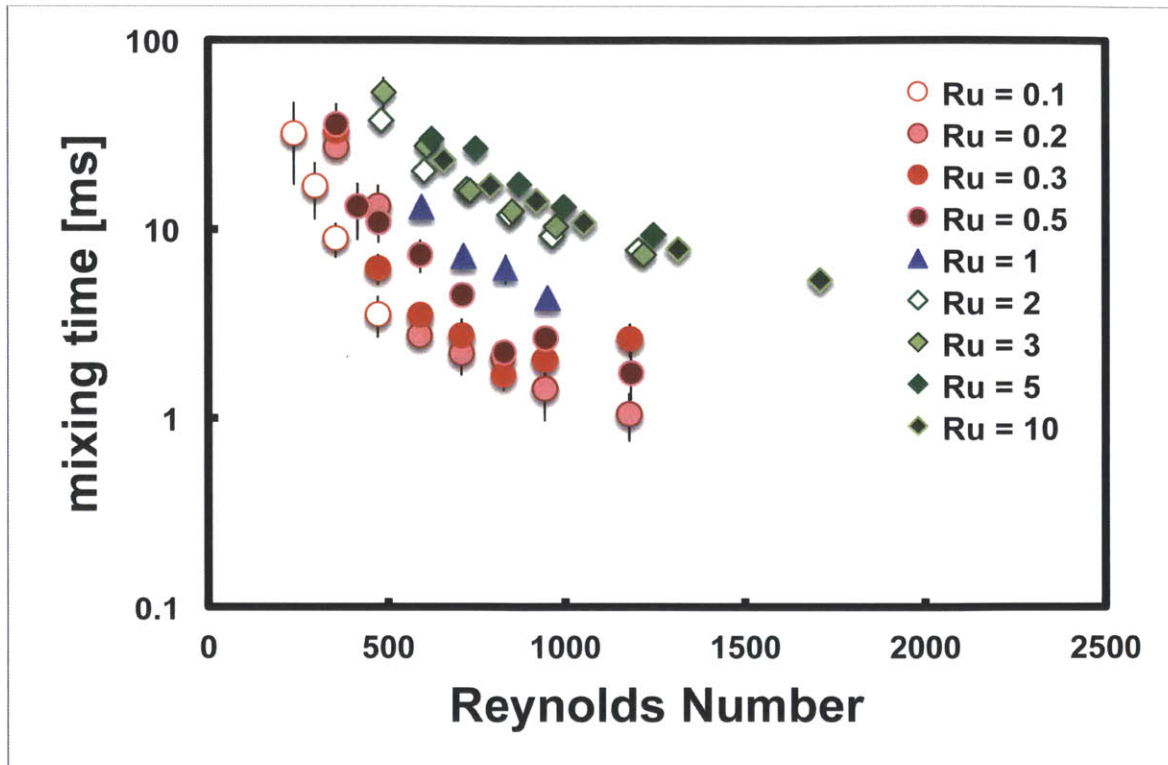


Figure 5: Mixing time data, plotted versus average-velocity Reynolds number Re_{ave} . Mixing times are averaged over multiple photographs. Error bars indicate one standard deviation. Absence of error bars indicates that the error bar is within the symbol size.

Mixing is clearly expedited as the Reynolds number increases, but the scaling is not obvious from the data presented in Figure 5.

The mixing time was non-dimensionalized by dividing it by τ_ω , given in (6). This dimensionless mixing time is plotted versus Re_{ave} in Figure 6.

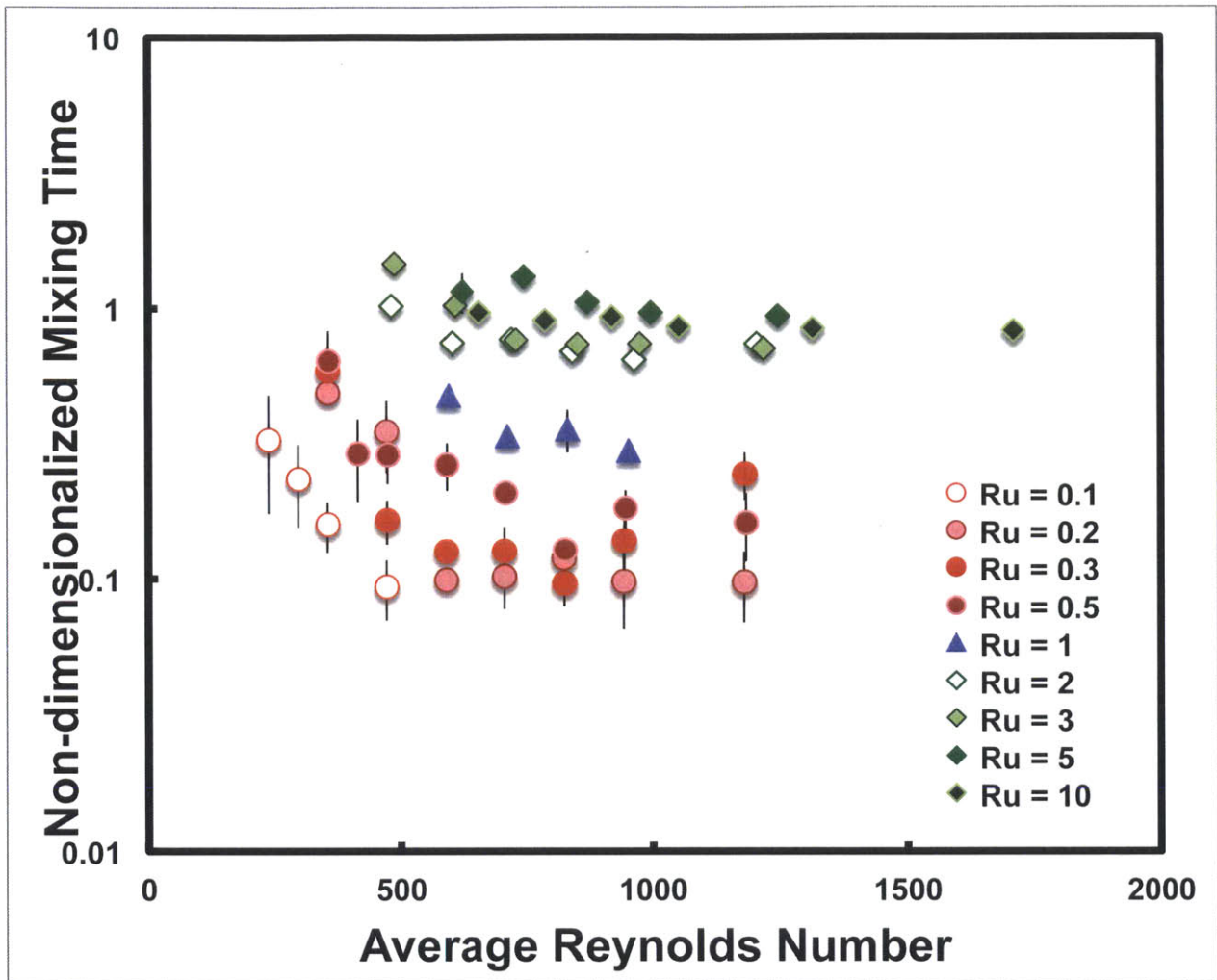


Figure 6: Mixing time, non-dimensionalized using τ_w . Error bars indicate one standard deviation. Absence of error bars indicates that the error bar is within the symbol size.

For velocity ratios $R_u > 1$, the data have more nearly collapsed onto the line $\frac{\tau_{mix}}{\tau_w} = 1$, especially at Re_{ave} above about 800. For these higher Reynolds numbers and flow rate ratios, the measured mixing time is within 40% of the predicted value. For $R_u \leq 1$, there is considerably more scatter. The flow in this region may be better described by another model that accounts for the vortices generated at the end of the inner tube.

4.3 Future Work

The low-Reynolds number, low-velocity ratio flows, which are believed to be dominated by flow focusing, can not be analyzed because mixing was not complete before the end of

the image. Additional experiments, designed to capture a longer distance, would allow investigation of the flow-focusing regime, which was not possible with the data collected in this project. The effect of the assumption in Equation (8), which was used to calculate mixing time, needs to be looked into.

Further investigation into mixing theory could shed light on the nature of the mixing at velocity ratios less than 1.

5. Conclusion

Mixing in the coaxial jet mixer was characterized based on experimentally determined mixing times. In the jetting regime, these mixing times were approximately consistent with those predicted by the EDD model.

7. Bibliography

1. Karnik, R.; Gu, F.; Basto, P.; Cannizzaro, C.; Dean, L.; Kyei-Manu, W.; Langer, R.; Farokhzad, O. C. Microfluidic Platform for Controlled Synthesis of Polymeric Nanoparticles. *Nano Lett.* **2008**, *8*, 2906–2912.
2. Rhee, M.; Valencia, P. M.; Rodriguez, M. I.; Langer, R.; Farokhzad, O. C.; Karnik, R. Synthesis of Size-Tunable Polymeric Nanoparticles Enabled by 3D Hydrodynamic Flow Focusing in Single-Layer Microchannels. *Adv. Mater.* **2011**, *23*, H79–H83.
3. Valencia, P. M.; Farokhzad, O. C.; Karnik, R.; Langer, R. Microfluidic Technologies for Accelerating the Clinical Translation of Nanoparticles. *Nat. Nanotechnol.* **2012**, *7*, 623–629.
4. Kim, B. Y. S.; Rutka, J. T.; Chan, W. C. W. Nanomedicine. *N. Engl. J. Med.* **2010**, *363*, 2434–2443.
5. Barreto, J. A.; O'Malley, W.; Kubeil, M.; Graham, B.; Stephan, H.; Spiccia, L. Nanomaterials: Applications in Cancer Imaging and Therapy. *Adv. Mater.* **2011**, *23*, H18–H40.
6. Qiao, R.; Yang, C.; Gao, M. Superparamagnetic Iron Oxide Nanoparticles: From Preparations to in Vivo MRI Applications. *J. Mater. Chem.* **2009**, *19*, 6274–6293.
7. Hrkach, J.; Hoff, D. V.; Ali, M. M.; Andrianova, E.; Auer, J.; Campbell, T.; Witt, D. D.; Figa, M.; Figueiredo, M.; Horhota, A.; *et al.* Preclinical Development and Clinical Translation of a PSMA-Targeted Docetaxel Nanoparticle with a Differentiated Pharmacological Profile. *Sci. Transl. Med.* **2012**, *4*, 128ra39–128ra39.
8. Vauthier, C.; Bouchemal, K. Methods for the Preparation and Manufacture of Polymeric Nanoparticles. *Pharm. Res.* **2009**, *26*, 1025–1058.
9. Fessi, H.; Puisieux, F.; Devissaguet, J. P.; Ammoury, N.; Benita, S. Nanocapsule Formation by Interfacial Polymer Deposition Following Solvent Displacement. *Int. J. Pharm.* **1989**, *55*, R1–R4.
10. Johnson, B. K.; Prud'homme, R. K. Mechanism for Rapid Self-Assembly of Block Copolymer Nanoparticles. *Phys. Rev. Lett.* **2003**, *91*, 118302.

11. Johnson, B. K.; Prud'homme, R. K. Chemical Processing and Micromixing in Confined Impinging Jets. *Aiche J.* **2003**, *49*, 2264–2282.
12. Kim, Y.; Chung, B. Lee; Ma, M.; Mulder, W. J. M.; Fayad, Z. A.; Farokhzad, O. C.; Langer, R. Mass Production and Size Control of Lipid–Polymer Hybrid Nanoparticles through Controlled Microvortices. *Nano Lett.* **2012**, *12*, 3587–3591.
13. Bałdyga, J.; Bourne, J. R. *Turbulent Mixing and Chemical Reactions*; Wiley, 1999.
14. Khattab, I. S.; Bandarkar, F.; Fakhree, M. A. A.; Jouyban, A. Density, Viscosity, and Surface Tension of Water+ethanol Mixtures from 293 to 323K. *Korean J. Chem. Eng.* **2012**, *29*, 812–817.
15. Warhaft, Z. Passive Scalars in Turbulent Flows. *Annu. Rev. Fluid Mech.* **2000**, *32*, 203–240.
16. Hughmark, G. A. Turbulence Properties in the Core of Pipe Flow. *Ind. Eng. Chem. Fundam.* **1977**, *16*, 307–308.